Check for updates

Domine, F., Belke-Brea, M., Bayle, A., Picard, G., Lévesque, E., & Kinnard, C. (2025). Challenges in Detecting High-Arctic Shrub Expansion From Optical Remote Sensing: Implications for Albedo and Climate Forcing. Journal of Geophysical Research: Biogeosciences, 130(10), Article e2024JG008593. https://doi.org/10.1029/2024JG008593 CC BY-NC-ND 4.0

JGR Biogeosciences

RESEARCH ARTICLE
10.1029/2024JG008593

Key Points:

- Field spectral measurements in the high-Arctic show shrubs have a lower albedo than prostrate vegetation but optical indices are similar
- Satellite remote sensing fails to detect shrubs in the high-Arctic using the most common optical index, normalized difference vegetation index
- Failure to detect shrubs in the high-Arctic misses a local positive climate feedback of 5.8 W m^{-2} due to the lower shrub albedo

Supporting Information:

Supporting Information may be found in the online version of this article.

Correspondence to:

F. Domine,
florent.domine@gmail.com

Citation:

Domine, F., Belke-Brea, M., Bayle, A., Picard, G., Lévesque, E., & Kinnard, C. (2025). Challenges in detecting high-Arctic shrub expansion from optical remote sensing: Implications for albedo and climate forcing. *Journal of Geophysical Research: Biogeosciences*, *130*, e2024JG008593. https://doi.org/10.1029/2024JG008593

Received 6 NOV 2024
Accepted 25 AUG 2025

Author Contributions:

Conceptualization: Florent Domine, Maria Belke-Brea, Christophe Kinnard
Data curation: Florent Domine, Maria Belke-Brea, Arthur Bayle, Christophe Kinnard
Formal analysis: Florent Domine, Arthur Bayle, Ghislain Picard, Christophe Kinnard
Funding acquisition: Florent Domine, Christophe Kinnard
Investigation: Maria Belke-Brea
Methodology: Maria Belke-Brea
Project administration: Florent Domine

© 2025. The Author(s).
This is an open access article under the terms of the Creative Commons Attribution-NonCommercial-NoDerivs License, which permits use and distribution in any medium, provided the original work is properly cited, the use is non-commercial and no modifications or adaptations are made.

Challenges in Detecting High-Arctic Shrub Expansion From Optical Remote Sensing: Implications for Albedo and Climate Forcing

Florent Domine[1,2,3,4], Maria Belke-Brea[1,2,3], Arthur Bayle[5], Ghislain Picard[6], Esther Lévesque[3,7], and Christophe Kinnard[3,7]

[1]Takuvik Joint International Laboratory, Université Laval, Québec City, QC, Canada, [2]CNRS-INSU, Paris, France, [3]Centre d'Études Nordiques, Université Laval, Québec City, QC, Canada, [4]Department of Chemistry, Université Laval, Québec City, QC, Canada, [5]Université Grenoble Alpes, Université Savoie Mont Blanc, CNRS, LECA, Grenoble, France, [6]Université Grenoble Alpes, CNRS, Institut des Géosciences de l'Environnement (IGE), UMR 5001, Grenoble, France, [7]Département des sciences de l'environnement, Université du Québec à Trois-Rivières, Trois-Rivières, QC, Canada

Abstract Climate change-induced shrub expansion in the Arctic feeds back on climate by reducing surface albedo. Vegetation dynamics are typically monitored by tracking the evolution of vegetation indices, such as normalized difference vegetation index (NDVI), derived from satellite imagery in processes known as greening or browning. However, detecting changes in vegetation type requires sufficient spectral variation. Here, we measured the spectral albedos (346–2,400 nm) of assemblages of prostrate vegetation and of the only erect shrub species *Salix richardsonii* on Bylot Island in the eastern Canadian high-Arctic to assess spectral differences among common vegetation types. The broadband albedo of *S. richardsonii* (0.132 ± 0.009) was lower than that of prostrate vegetation (0.166 ± 0.008). However, NDVI values showed no significant difference (0.598 ± 0.074 vs. 0.561 ± 0.021). Satellite remote sensing using NDVI with spatial resolutions from 0.5 to 30 m using Pléiades, Sentinel-2 and Landsat-8 failed to detect differences in reflectance and NDVI between prostrate vegetation and *S. richardsonii*. These findings suggest that long-term NDVI trend analysis may be insufficient to capture the structural vegetation shift in these climate-sensitive areas. Failure to detect erect shrub expansion in the high-Arctic may therefore omit a climate change effect which produces a surface albedo decrease of 0.03 and a local summer solar forcing of 5.8 W m^{-2}.

Plain Language Summary With climate change, taller shrubs are replacing tundra vegetation in the Arctic. Shrubs reflect less sunlight than tundra vegetation: they have a lower albedo. Shrub expansion thus contributes to further warming, creating positive feedback on climate, which must be measured to improve climate models. Shrub expansion across the Arctic is usually monitored using satellite remote sensing in the visible and infrared ranges. Because satellites only monitor a limited number of wavelengths, indices combining several wavelengths are used to track vegetation changes. The most commonly used index is called Normalized difference vegetation index (NDVI). Here we use both field measurements, which allow shrub detection with certainty, and satellite data to test whether satellites can accurately detect shrub expansion in the high-Arctic. We show that, in the field, shrubs have NDVI values similar to low vegetation. NDVI from satellite also fails to distinguish shrubs from low vegetation. However, our field measurements show that shrubs in the high-Arctic have an albedo of 0.132, compared to 0.166 for low vegetation. This difference creates a local surface forcing of 5.8 W m^{-2}. In comparison, the global forcing due to anthropogenic CO_2 is about 2.3 W m^{-2}. Common shrub detection methods in the high-Arctic therefore miss an important local climate forcing.

1. Introduction

With climate change, increases in Arctic vegetation greenness and primary productivity are observed in many locations (Bayle et al., 2022; Berner et al., 2020; Boelman et al., 2011; Frost et al., 2025; Gauthier et al., 2013; Ju & Masek, 2016). Erect shrubs (>30 cm) (Myers-Smith et al., 2015) are the tallest growth form above the treeline and their increase in abundance, a.k.a. shrub expansion or shrubification (Myers-Smith, Forbes, et al., 2011), has been reported repeatedly near treeline (Buchkowski et al., 2020; Ropars & Boudreau, 2012; Sturm et al., 2001), with complex effects on the energy budgets at the top of the vegetation and at the ground surface, therefore impacting the near surface air and ground temperatures (Bonfils et al., 2012; Kropp et al., 2021; Rydsaa et al., 2015).

21698961, 2025, 10, Downloaded from https://agupubs.onlinelibrary.wiley.com/doi/10.1029/2024JG008593 by Universitaet Du Quebec A Trois Rivieres, Wiley Online Library on [11/02/2026]. See the Terms and Conditions (https://onlinelibrary.wiley.com/terms-and-conditions) on Wiley Online Library for rules of use; OA articles are governed by the applicable Creative Commons License

Software: Arthur Bayle, Christophe Kinnard
Supervision: Florent Domine
Writing – original draft: Florent Domine, Arthur Bayle, Christophe Kinnard
Writing – review & editing: Ghislain Picard, Esther Lévesque

The presence of erect shrubs has been used to delineate the limit between the low- and high-Arctic (Bliss & Matveyeva, 1992; Walker et al., 2005). Yet, isolated populations can be found in protected areas north of this arbitrary line (Jacobs et al., 1997). Most of the vegetation in the high-Arctic grows within a few centimeters of the ground including the dominant prostrate shrubs (*Salix arctica, Dryas integrifolia*, and *Cassiope tetragona*). The presence of erect shrubs (rarely taller than 50 cm) in these landscapes has the potential to transform ecosystems by decreasing the albedo and warming the surface (Aartsma et al., 2020; Blok et al., 2011; Domine, Bayle, et al., 2025; Juszak et al., 2014), insulating the ground with metamorphized snow (Domine et al., 2016) and by modifying trophic interactions (Poirier et al., 2023), carbon sequestration (Lamarque et al., 2023; Ola et al., 2022) and energy budgets (J. Chen et al., 2022; Lafleur & Humphreys, 2018). There is therefore a strong interest to assess erect shrub dynamics in these remote and rapidly changing environments (Beringer et al., 2005; Frost et al., 2025; Juszak et al., 2017).

The most obvious effect of the presence of erect shrubs on the summer energy budget at the top of the vegetation is on shortwave radiation, via changes in broadband (BB) albedo. Field studies have indeed found that the BB albedo of erect shrubs is significantly lower than that of prostrate vegetation in boreal and low-Arctic regions (Aartsma et al., 2020; Beringer et al., 2005; Blok et al., 2011; Domine, Bayle, et al., 2025; Juszak et al., 2014; Nicholls & Carey, 2021; Ramtvedt et al., 2021). For example, a comparison of the BB albedo of lichen heath and shrubs (*Betula nana*) in Southern Norway revealed values of 0.255 for lichen and 0.132 for shrubs (Aartsma et al., 2020), leading to a 16% increase of the solar energy absorbed by the surface if shrubs replace lichen. Inversely, the decrease in shrub height and abundance caused by reindeer grazing has been found to increase surface albedo (te Beest et al., 2016).

All these studies have however taken place near tree lines or in the low-Arctic, with hardly any studies of the impact of shrubs on albedo in the high-Arctic. For evaluating circumarctic effects, the presence of shrubs must first be detected using remote sensing. A widely used method is the normalized difference vegetation index (NDVI), which has been found to be correlated with biomass and the leaf area index (LAI) in the Arctic (Berner et al., 2018; Rees et al., 2020). Taller vegetation, which generally has a greater biomass and LAI, has higher NDVI values (Blok et al., 2011; Boelman et al., 2011; Juszak et al., 2014; Pattison et al., 2015), and this property has often been used to attribute greening trends, that is, increases in NDVI, to changes in vegetation assemblages toward tall shrubs in the Arctic (Jespersen et al., 2023; Rees et al., 2020). However, at Herschel Island (69°N, western Canadian Arctic), (Cunliffe et al., 2020) concluded that "Vegetation 'greenness' measured as NDVI across four independent multispectral surveys explained only a small proportion of the variability in the biomass of vascular plants and was influenced by moss cover, suggesting caution should be used when attributing differences in NDVI to differences in either vascular plant biomass or phytomass." Therefore, further tests of the detectability of Arctic shrubs using NDVI appear useful.

Regarding terrestrial Arctic albedo, remote sensing studies of this variable have in general concluded that it has been decreasing in most summer months except July (Plekhanova et al., 2022; Webb et al., 2021; Yu et al., 2022). The slight July increase in albedo has been tentatively attributed to a decrease in surface water (Plekhanova et al., 2022; Webb et al., 2021). The overall albedo decrease seems mostly consistent with local field studies observing increasing shrub abundance (Forbes et al., 2010; Fraser et al., 2014; Frost & Epstein, 2014; Mekonnen et al., 2021). However, shrubification is only one of the possible causes of albedo change. Other causes such as fire, post-fire recovery and increase in surface water (Webb et al., 2021) can lead to increases or decreases in albedo so that identifying the contribution of shrubification is uncertain using remote sensing alone, especially considering the potential difficulty in identifying shrub presence using indices such as NDVI (Cunliffe et al., 2020). Therefore, the combination of field studies and remote sensing in the high-Arctic is required to: (a) test the possibility to detect shrubs by remote sensing methods and (b) quantify the impact of shrubification on albedo.

To address both these questions, we combined field work with remote sensing on Bylot Island (73°N, 80°W) and northern Baffin Island. In this Canadian high-Arctic region, *Salix richardsonii* is the only truly erect species. There, this shrub remains small (generally <50 cm) with a fairly open structure and few leaves which are insufficient to conceal the ground or understory vegetation. This contrasts with canopy-forming shrubs (Myers-Smith et al., 2015) further south such as dwarf birch, which have a fairly high LAI (Chang et al., 2022) and through which the ground is much less visible. This raises the question of whether *S. richardsonii* at Bylot Island can be detected through optical remote sensing using albedo or indices such as NDVI, or simple reflectance

21698961, 2025, 10, Downloaded from https://agupubs.onlinelibrary.wiley.com/doi/10.1029/2024JG008593 by Universitaet Du Quebec A Trois Rivieres, Wiley Online Library on [11/02/2026]. See the Terms and Conditions (https://onlinelibrary.wiley.com/terms-and-conditions) on Wiley Online Library for rules of use; OA articles are governed by the applicable Creative Commons License

at specific wavelengths, and whether its expansion can be tracked by analyzing NDVI trends over decades. Another question is whether such shrubs have a significant impact on albedo. We have therefore measured in the field the spectral albedos of numerous spots ($n = 83$) at locations featuring a wide variety of vegetation covers. These data were used to compare NDVI and BB albedo values of prostrate vegetation and of *S. richardsonii*. We then determined NDVI using remote sensing methods over a wide range of spatial resolutions by assembling a multiscale remote sensing data set using an unmanned aerial vehicle (UAV, 0.3 m resolution) and data from the satellites Pléiades (0.5 m), Sentinel-2 (10 m) and Landsat-8 (30 m).

2. Methods

2.1. Site Description

Field measurements were performed in Qarlikturvik valley (73.15°N, 80.00°W) on Bylot Island, North of Baffin Island in the Canadian Arctic Archipelago (Figure 1). A few measurements were also performed at Mala River Valley (73.01°N, 80.69°W) on northern Baffin Island just across Navy Board Inlet from Bylot Island (Figure 1). Table 1 lists the location of the field spectral measurements and describes the vegetation assemblages. A wide range of vegetation types are found because of the presence of humid, moist and mesic areas, as well as the presence of alluvial fans with active and inactive flow channels (Lamarque et al., 2023; Ola et al., 2022). A mixture of mosses, lichens, graminoids and forbs are observed along with prostrate shrub species such as *Salix arctica, S. reticulata, S. herbacea*, *Dryas integrifolia*, and *Cassiope tetragona* as detailed by Gauthier et al. (2011). Although *S. arctica* occasionally reaches heights around 10 cm, the only erect shrub species is *S. richardsonii*, usually around 40–50 cm tall. It is commonly found in alluvial fans, where spring water flow, sediment deposition, and active layer depth are most important (Lamarque et al., 2023). There, large fairly homogeneous patches with individuals reaching 50 cm in height and covering several 1,000 m^2 are observed. The understory below these large patches usually consists mostly of mosses, graminoids, *S. arctica*, and bare soil patches. In less active parts of the alluvial fans and in riparian areas, and sometimes in mesic areas, smaller patches of about 10 m in their largest dimension are occasionally observed. The shrubs there are shorter and have sparser cover than in more active areas. Although LAI was not quantitatively measured, a visual inspection indicates that the LAI of taller shrubs in active parts of alluvial fans is greater than in less active parts, in line with previous findings (Lamarque et al., 2023). Figure 2 presents overview photographs illustrating prostrate vegetation and *S. richardsonii* patches. In this study, prostrate vegetation includes prostrate shrubs, herbaceous vegetation, mosses and lichens. Figures S1 and S2 in Supporting Information S1 show close-up photographs of the main vegetation assemblages studied. Mosses showed large appearance variations, from brown mesic mosses to bright green humid mosses (Figure S3 in Supporting Information S1).

2.2. Spectral Albedo Measurements

Spectral albedo was measured with a field portable spectroradiometer (HR-1024 model, Spectra Vista Corporation, SVC) between 10 and 18 July 2015, between about 10:30 and 16:30 local summer time each day so that the solar zenith angle (SZA) varied between 50.1 and 60.3°. Summer 2015 was drier than most summers in terms of precipitation and soil moisture. Over the 2013–2019 period, it was the driest summer (Domine et al., 2021), raising the question of whether these dry conditions may have led to atypical NDVI values. Indeed, remote sensing studies indicate that soil moisture and NDVI are often anticorrelated (T. Chen et al., 2014). However, field studies at 0.5 m spatial resolution are less conclusive (Engstrom et al., 2008). At the time of measurements, shrub foliage was fully developed. Time-lapse images at the SALIX-D1 location (Figure S4 in Supporting Information S1) do not reveal any significant further foliage development after mid-July. A comparison of time-lapse images of years 2015–2024 do not reveal any striking difference in greenness or foliage development between years. These observations support our assumption that despite the relative dryness of summer 2015, NDVI values were not significantly affected. Yellow leaves were visible starting on 4 August 2015. Lighting conditions during spectra recording were mostly clear sky to nearly clear sky ($n = 78$). A few spectra ($n = 5$) were measured under completely overcast conditions on 16 July. Clouds were then cirrostratus and stratus, optically thick with no visible shadows. The light collector connected to the spectrometer was an SVC full sky irradiance integrating sphere 7.5 cm in inner diameter with a nadir to 85° field of view, making it a nearly perfect cosine receptor. It was located at the end of a 2-m metal rod resting on a tripod, at a height of about 1.2 m (Figure S5 in Supporting Information S1), so that 71% of the radiance entering the sphere comes from a circle 1.2 m in radius below the sphere. For measurements above 40 cm shrubs, this radius is reduced to 0.8 m. Albedo was determined

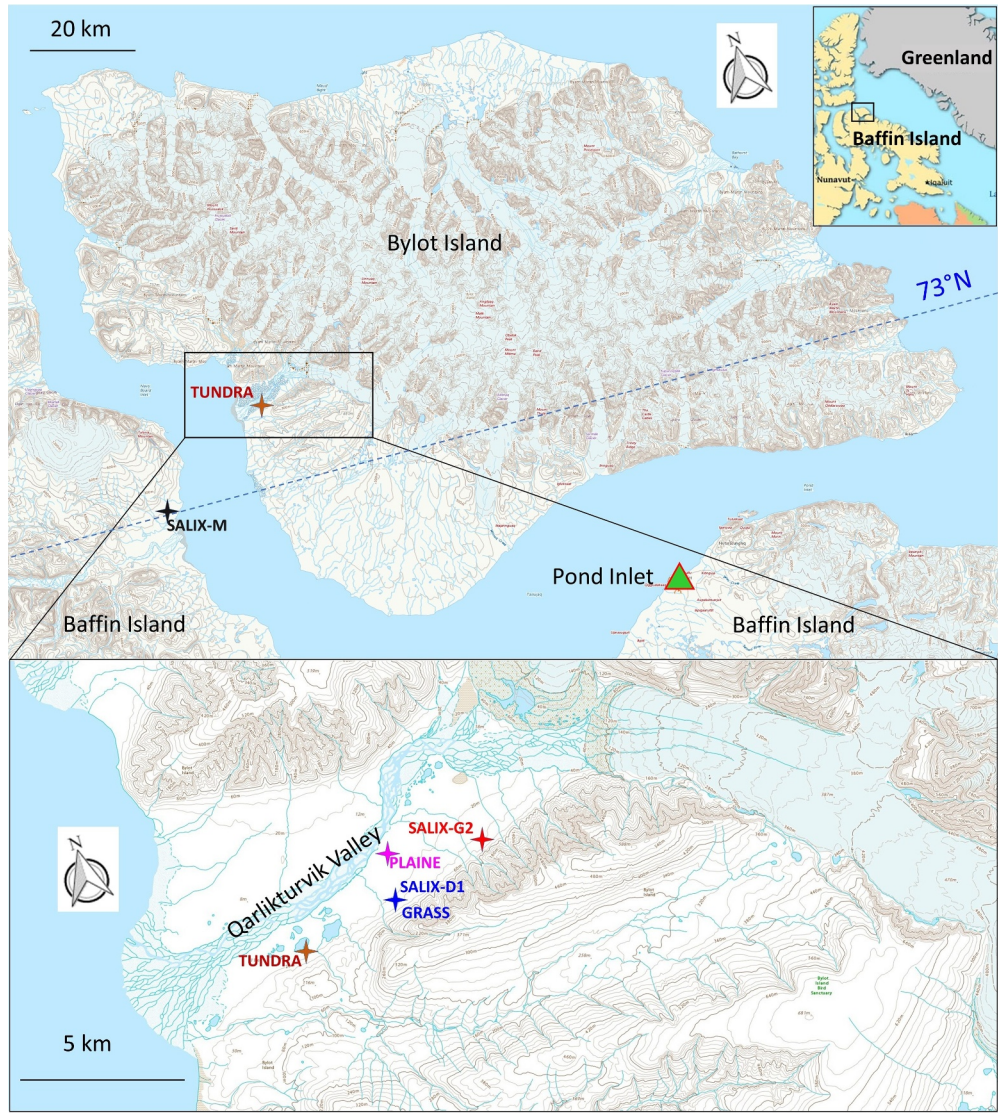

Figure 1. Location of Qarlikturvik valley on Bylot Island in the Canadian high-Arctic. Stars indicate where spectra were acquired. Note the SALIX-M site on Baffin Island, in Mala River valley on the top map, where spectra were also acquired. The nearest community, Pond Inlet (Nunavut), is indicated by a triangle. Maps from https://search.open.canada.ca/openmap/8ba2aa2a-7bb9-4448-b4d7-f164409fe056, last accessed on 16 November 2022.

from successive measurements of the downwelling and upwelling radiation, by rotating the metal rod 180° between both measurements. The horizontality of the sphere was checked with an electronic inclinometer located next to the sphere. The spectrometer dark current was measured automatically before each measurement and automatically subtracted from the measurement. A photodiode monitored the solar irradiance and data where irradiance varied by >1% between both measurements were rejected, as detailed earlier (Belke-Brea et al., 2020). To cover a large part of the solar spectrum, the spectrometer is composed of three independent optical lines, with their specific gratings and light detectors. The spectral resolution varies between 1 and 1.5 nm for the Si detector (346.5–982 nm), 3.5–4 nm for the first InGaAs detector (982–1,883 nm) and 2.5 nm for the second InGaAs detector (1,883–2,514 nm). For each spectrum, a running mean average was used to improve the signal-to-noise ratio. Averaging was over a 12 nm range from 346.5 to 1,800 nm, and 80 nm beyond that. In general data quality for wavelengths greater than 2,400 nm was poor due to low irradiance and thus unreliable for BB albedo calculation. We therefore only present data over the 346.5–2,400 nm range. The impact of neglecting the 2,400–2,514 nm range is negligible for BB albedo calculations, because the fraction of downwelling solar energy within

21698961, 2025, 10, Downloaded from https://agupubs.onlinelibrary.wiley.com/doi/10.1029/2024JG008593 by Universitaet Du Quebec A Trois Rivieres, Wiley Online Library on [11/02/2026]. See the Terms and Conditions (https://onlinelibrary.wiley.com/terms-and-conditions) on Wiley Online Library for rules of use; OA articles are governed by the applicable Creative Commons License

Table 1
Main Characteristics of the Locations Where Spectral Albedo Measurement Were Performed

Location	Latitude	Longitude	Vegetation types found	Veg. height (cm)
TUNDRA	73.150°	−80.004°	Humid and moist polygons with prostrate vegetation with mostly mosses, graminoids, *Salix arctica* and *Salix herbacea*	5
PLAINE	73.167°	−79.915°	Prostrate vegetation and bare soil patches caused by cryoturbation (mudboils) with mosses, graminoids and *S. arctica*	5
GRASS	73.158°	−79.907°	Prostrate vegetation between patches of *Salix richardsonii* dominated by *S. arctica*, with litter, mosses, graminoids and occasional bare soil	8
SALIX-D1	73.158°	−79.907°	Scattered patches of *S. richardsonii*. Understory includes mosses, graminoids, litter, *S. arctica* and bare soil	35
SALIX-M	73.006°	−80.685°	Mesic area with patches of *S. richardsonii*. Understory includes mosses, graminoids and litter. Between patches: herb tundra with graminoids and mosses. The area is not within an alluvial fan	40
SALIX-G2	73.168°	−79.812°	Extended area in an alluvial fan with *S. richardsonii*. Understory includes litter, mosses, graminoids, bare soil, *S. arctica* and *S. reticulata*	50

Note. The coordinates are those of the center of the areas studied, where several spectra were acquired within 50 m of the positions indicated. GRASS and SALIX-D1 have the same coordinates because the area was a mix of *S. richardsonii* and prostrate vegetation.

that range was on average 0.35% only. BB Albedos calculated with the reduced and full ranges differed by less than 0.0005, and using the reduced range is certainly more reliable.

Finally, we corrected for the lack of data in the 300–346.5 nm range to calculate the BB albedo. The downwelling energy contribution in this range was evaluated using the SMARTS radiation model (https://www.nrel.gov/grid/solar-resource/smarts.html, last accessed on 6 June 2023). For SZAs in the ranges of interest here and over vegetated surfaces, this wavelength range contributes about 1.6% to the total downwelling radiation under clear sky conditions. The albedo of vegetation surfaces in the 300–340 nm range has been reported to be about 90% of that at 350 nm for the vegetation covers studied (Feister & Grewe, 1995). We therefore correct for the lack of the 300–346.5 nm range by assuming that (a) 1.6% of incident irradiance is in that range; (b) the average albedo over that range is 0.9 × albedo measured at the lowest available wavelength: 346.5 nm.

Spectral albedo was measured over different surfaces dominated by (a) mudboils, $n = 4$; (b) graminoids, $n = 7$; (c) mosses, $n = 17$; (d) *S. arctica*, $n = 16$; (e) three groups of *S. richardsonii* located in different areas, $n = 34$ under clear sky conditions and $n = 5$ under overcast conditions (Table 2). We used spectral albedo measured in either lighting condition to calculate BB albedo under both (a) clear sky; and (b) overcast conditions. To be rigorously comparable, all BB albedo calculations must use the same spectral irradiance distributions. We implicitly assume that the difference of directionality between the various measurements had a second order effect relative to the

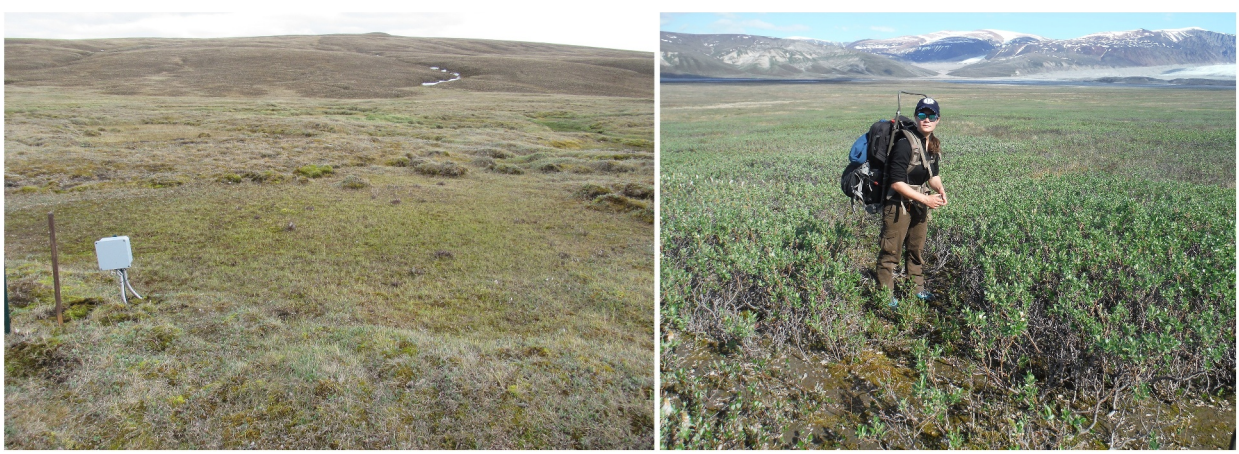

Figure 2. Typical prostrate vegetation near TUNDRA (left) and a patch of *Salix richardsonii* near SALIX-G2 (right). The person is about 1.62 m tall.

21698961, 2025, 10, Downloaded from https://agupubs.onlinelibrary.wiley.com/doi/10.1029/2024JG008593 by Universitaet Du Quebec A Trois Rivieres, Wiley Online Library on [11/02/2026]. See the Terms and Conditions (https://onlinelibrary.wiley.com/terms-and-conditions) on Wiley Online Library for rules of use; OA articles are governed by the applicable Creative Commons License

21698961, 2025, 10, Downloaded from https://agupubs.onlinelibrary.wiley.com/doi/10.1029/2024JG008593 by Universitaet Du Quebec A Trois Rivieres, Wiley Online Library on [11/02/2026]. See the Terms and Conditions (https://onlinelibrary.wiley.com/terms-and-conditions) on Wiley Online Library for rules of use; OA articles are governed by the applicable Creative Commons License

Table 2
Broadband Albedo (300–2,400 nm) and Normalized Difference Vegetation Index of the Dominant Vegetation Cover Types

Dominant cover type	Locations	Number of spectra, *n*	BB albedo		NDVI
			Clear sky	Overcast	
Erect vegetation					
S. richardsonii	SALIX-D1	17	0.148 ± 0.017	0.139 ± 0.015	0.599 ± 0.026
S. richardsonii	SALIX-M	8	0.140 ± 0.017	0.129 ± 0.015	0.517 ± 0.038
S. richardsonii	SALIX-G2	14	0.113 ± 0.023	0.108 ± 0.021	0.633 ± 0.023
Prostrate vegetation					
S. arctica	GRASS	16	0.183 ± 0.019	0.169 ± 0.018	0.591 ± 0.034
Graminoids	TUNDRA, SALIX-M	7	0.162 ± 0.037	0.150 ± 0.035	0.517 ± 0.084
Mosses	TUNDRA, PLAINE	17	0.153 ± 0.017	0.140 ± 0.016	0.542 ± 0.058
Mudboils	PLAINE, SALIX-G2	4	0.136 ± 0.013	0.125 ± 0.013	0.501 ± 0.038
Data by main types (prostrate vs. *S. richardsonii*)					
S. richardsonii		39	0.134 ± 0.026	0.126 ± 0.023	0.594 ± 0.054
Prostrate vegetation		44	0.166 ± 0.026	0.153 ± 0.024	0.552 ± 0.064

Note. BB albedos have been calculated for both clear sky and overcast conditions. The standard deviations are indicated.

spectral distribution difference (Sandmeier et al., 1999). For the clear sky downwelling irradiance distribution, we used the average of five spectra measured over representative surfaces (two for *S. richardsonii*, two over mosses, one over mudboil, measured between 12:00 and 16:00 on 11, 13, and 15 July). For the overcast downwelling irradiance distribution, we used the five spectra measured on 16 July, which were all very similar. Both normalized irradiance distributions are shown in Figure S6 in Supporting Information S1. As expected, the downwelling irradiance in cloudy conditions is depleted in the near and short-wave infrared.

2.3. NDVI Calculations From Ground Spectral Data

NDVI uses red (*R*) and near-infrared (NIR) spectral ranges. Different spectral ranges are used in the literature for *R* and NIR, depending on the satellite used when NDVI is determined from remote sensing data (Berner et al., 2020; Blok et al., 2011; Juszak et al., 2014), or on the portable instrument used when it is determined from field data (Boelman et al., 2011; Jespersen et al., 2023; May et al., 2022). Here we use wavelengths centered on the Landsat *R* and NIR bands:

$$\mathrm{NDVI} = (\mathrm{NIR}_{865} - R_{655})/(\mathrm{NIR}_{865} + R_{655}) \quad (1)$$

Since our spectra are smoothed over 12 nm, in terms of raw data the ranges are *R* (649–661) and NIR (859–871). Both these ranges are also within the ranges of the Pléiades satellite *R* (620–700) and NIR (775–915) bands.

2.4. NDVI Calculations From Remote Sensing Data

In addition to ground spectral measurements, we gathered July remote sensing acquisitions from four independent sources, each with a specific spatial resolution: a UAV (0.3 m), Pléiades-1B (0.5 m), Sentinel-2 (10 m) and Landsat-8 (30 m). For each sensor, we computed NDVI using their respective NIR and *R* bands following Equation 1 to test whether erect shrubs have specific radiometric signals at multiple scales. Data were acquired in different years because of logistical constraints or quality data availability for July. However, we essentially focus on differences in optical responses between *S. richardsonii* and prostrate vegetation for any given sensor. Observations and time-lapse cameras do not reveal any significant difference in vegetation development from year to year. We therefore estimate that using data from different years does not affect our conclusions.

Regarding the UAV, a 3.6 km^2 zone near SALIX-D1 and with patchy *S. richardsonii* coverage was surveyed with a fixed wing Ebee X mapping UAV on 16 July 2022. The UAV was equipped with a Duet M multispectral camera, which combines a Parrot Sequoia + sensor for multispectral imaging and a Sensefly S.O.D.A. sensor for

21698961, 2025, 10, Downloaded from https://agupubs.onlinelibrary.wiley.com/doi/10.1029/2024JG008593 by Universitaet Du Quebec A Trois Rivieres, Wiley Online Library on [11/02/2026]. See the Terms and Conditions (https://onlinelibrary.wiley.com/terms-and-conditions) on Wiley Online Library for rules of use; OA articles are governed by the applicable Creative Commons License

RGB imaging. The Sequoia + sensor is composed of four distinct sensors in the green (550 ± 40 nm), red (660 ± 40 nm), red-edge (735 ± 10 nm), and near-infrared (790 ± 40 nm) bands. The UAV was flown with side and frontal overlaps between the images of 70% and 87%, respectively. The Duet M camera is equipped with a sunshine sensor, which corrects variations in illumination. This eliminates the need for a radiometric calibration target on the ground (Cubero-Castan et al., 2018). The RGB and multispectral images were processed in Pix4dMapper version 4.8.4 to produce RGB and spectral reflectance orthoimages with 6.78 and 30 cm spatial resolution, respectively. Three ground control points (GCPs) were distributed over the surveyed area to validate the accuracy of the direct georeferencing. Both the UAV images and GCPs were geolocated precisely using post-processing kinematics (PPK) relative to a fixed GNSS base station installed near the camp, whose coordinates were precisely calculated using precise point positioning (PPP) for several long occupation times (>5 hr). The root-mean-squared (RMS) horizontal geolocation accuracy of the orthoimages products derived from the GCPs was ±5 cm.

Regarding the Pléiade-1B satellite, a stereo pair of 5-band (B, G, R, NIR: 2 m resolution; panchromatic: 0.5 m resolution) images from 28 July 2016 was obtained. Spectral ranges are 430–550 nm (blue), 500–620 nm (green), 590–710 (red) and 740–940 nm (NIR) and 480–830 nm (panchromatic). The raw images Digital Numbers (DN) were converted to ground reflectance with ATCOR (Atmospheric & Topographic Correction) in the Catalyst Professional® software, version 2223.0.2 (PCI Geomatics). ATCOR is an atmospheric correction algorithm that reduces the influence of the atmosphere (water vapor and aerosol type), solar illumination, sensor viewing geometry, and terrain illumination on the DNs of the raw satellite optical images, using the MODTRAN 5 radiation transfer model (Richter & Schläpfer, 2017; Richter, Schläpfer, & Müller, 2006). The reflectance images were orthorectified using a 2 m DEM derived from the panchromatic stereo pair (Mohammadzadeh Khani et al., 2023). The native geolocation accuracy is 4.5 m for Pléiades-1B without GCPs (Lebègue et al., 2013). To improve the geolocation accuracy of the Pléiades products, GCPs were collected automatically from the UAV RGB orthoimage from 16 July 2022, which was approximately centered on the sector of interest where manual shrubs surveys were performed (Figure 3). The RGB orthoimage was first aggregated to 10 cm resolution to speed up the process. Automatic GCP collection was performed in Catalyst Professional®, based on image correlation between the reference UAV RGB orthoimage and the panchromatic and multispectral images, using Fast Fourier Transform phase matching. 87 and 82 GCPs regularly distributed within the area common to the UAV and Pléiades image were found for the panchromatic and multispectral images, respectively. The GCPs were used to compute and apply a first order adjustment to the rational polynomial coefficient (RPC) model provided with the Pléiades image, resulting in a horizontal geolocation residual RMS error of 3.2 and 2.6 cm for the panchromatic and multispectral images, respectively. The multispectral image was then pan-sharpened using the MRAFUSION algorithm in Catalyst Professional®. MRAFUSION is a multi-resolution algorithm that fuses black-and-white panchromatic and multispectral color images using wavelet decomposition, providing similar-to-superior results than traditional pan sharpening approaches while preserving the spectral characteristics of the original images (González-Audícana et al., 2005). This allowed improving the spectral bands from their native spatial resolution (2 m) to the higher resolution of the panchromatic band (0.5 m), which is better suited to capture reflectance contrasts within heterogeneous shrub patches.

The Sentinel-2B product is a surface reflectance level of correction (2A) acquisition from 26 July 2019 with neither clouds nor cloud shadows over our study area, processed using the Multi-Temporal Cloud Screening and Atmospheric Correction software (MAJA) (Colin et al., 2023) and downloaded from theia.cnes.fr, last accessed on 02 May 2024. NDVI was computed using bands 4 (red, 633–695 nm) and 8 (NIR, 726–938 nm).

The Landsat-8 OLI image used is a Tier 1 Collection 2 acquisition from 23 July 2015 with neither clouds nor cloud shadows over our study area and a geometric RMSE model of 5.024 m, with a surface reflectance level of correction (2A) downloaded from earthexplorer.usgs.gov (Last accessed on 03 May 2024). NDVI was computed using bands 4 (red, 630–680 nm) and 5 (NIR, 845–885 nm).

Finally, to test the potential impact of our findings at the scale of the Canadian high-Arctic, we used Google Earth Engine (GEE) to produce a 10-m Sentinel-2 based map of July NDVI for the Canadian high-Arctic. We gathered all available images from the Sentinel-2 Level-2A collection of July, years 2017–2023, and masked clouds and cloud shadows using the S2 cloud probability collection with a probability threshold of 80%. NDVI was computed on each cloud-free image and pixelwise median was computed to obtain a median value of NDVI for the month of July.

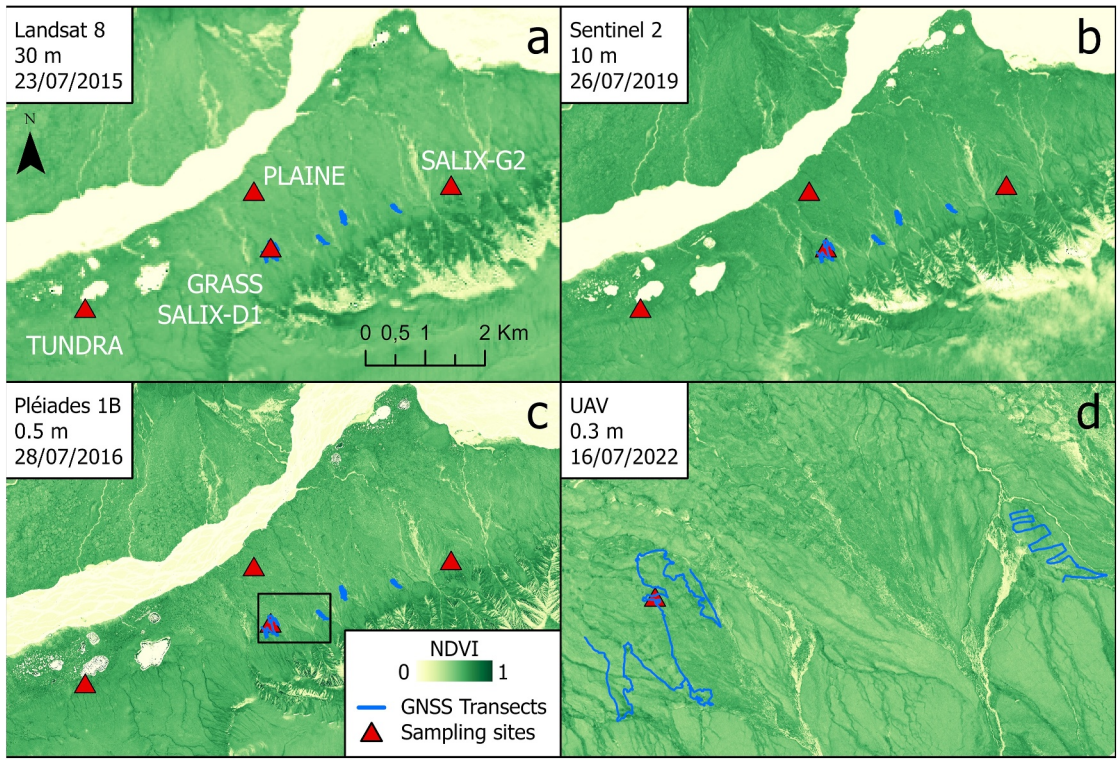

Figure 3. Normalized difference vegetation index map from (a) Landsat-8, (b) Sentinel-2, (c) Pléiades-1B, and (d) drone acquisitions over our study site showing the location of GNSS shrub survey transects, and the location of the sites with spectrometer measurements with associated names. The black frame in (c) is the area of the unmanned aerial vehicle survey in (d).

2.5. Reflectance Extraction Along Shrub Transects and Sites

For reflectance comparison between *S. richardsonii* and prostrate vegetation, GNSS field surveys were conducted in summer 2023 to map erect shrubs along transects with a spatial resolution equal to or better than the resolution of Pleiades (<0.5 m). The shrub transects were walked with a GNSS in dynamic mode, sampling the position at each second. When entering and exiting an isolated *S. richardsonii* shrub or a continuous patch of shrubs, the code "A" was noted along with the GNSS counter. Later, points in between "A"-coded time stamps were given the "A" value, all others the "S" value ("soil"). GNSS surveys were post-processed with PPK relative to the same fixed base station used for georeferencing the UAV. The point shrub survey data was converted to two-class (shrub, no-shrub) polyline objects (Figure S7 in Supporting Information S1) representing the abundance of erect shrub *S. richardsonii*.

The proportion of the transect line pertaining to the erect shrub class within a given image pixel was calculated using the Line Statistic tool in Arcgis Spatial Analyst, using search distances of 0.20 m (UAV), 0.41 m (Pléiades), 5 m (Sentinel-2), and 15 m (Landsat-8). For the high-resolution UAV and Pléiades images, these distances correspond to the distance between a cell center point and its corners plus a 95% confidence horizontal pixel geolocation uncertainty estimated as twice the typical orthorectification RMS error of 3 cm. This error was ignored for the coarser Sentinel-2 and Landsat-8 images. For Sentinel-2, Pléiades-1B and UAV, a given pixel was considered as erect or prostrate only if 100% of the transect lines within the pixel was of one of the classes. For the coarser resolution Landsat-8, we used a threshold of <25% and >75% of erect shrubs to classify as either prostrate or erect vegetation to maximize the number of samples. This approach implicitly assumes that the composition of transect lines within a pixel reflects the areal composition. In large alluvial fan patches, this assumption is likely valid. For smaller isolated patches, whose size is typically about 10 m, the assumption is likely valid for UAV and Pléiades data (resolutions 0.3 and 0.5 m). For Sentinel-2 (10 m resolution), it is probably reasonably valid. For Landsat-8 (resolution 30 m) the validity may not be as good and the 25%–75% range was set in an attempt to

21698961, 2025, 10, Downloaded from https://agupubs.onlinelibrary.wiley.com/doi/10.1029/2024JG008593 by Universitaet Du Quebec A Trois Rivieres, Wiley Online Library on [11/02/2026]. See the Terms and Conditions (https://onlinelibrary.wiley.com/terms-and-conditions) on Wiley Online Library for rules of use; OA articles are governed by the applicable Creative Commons License

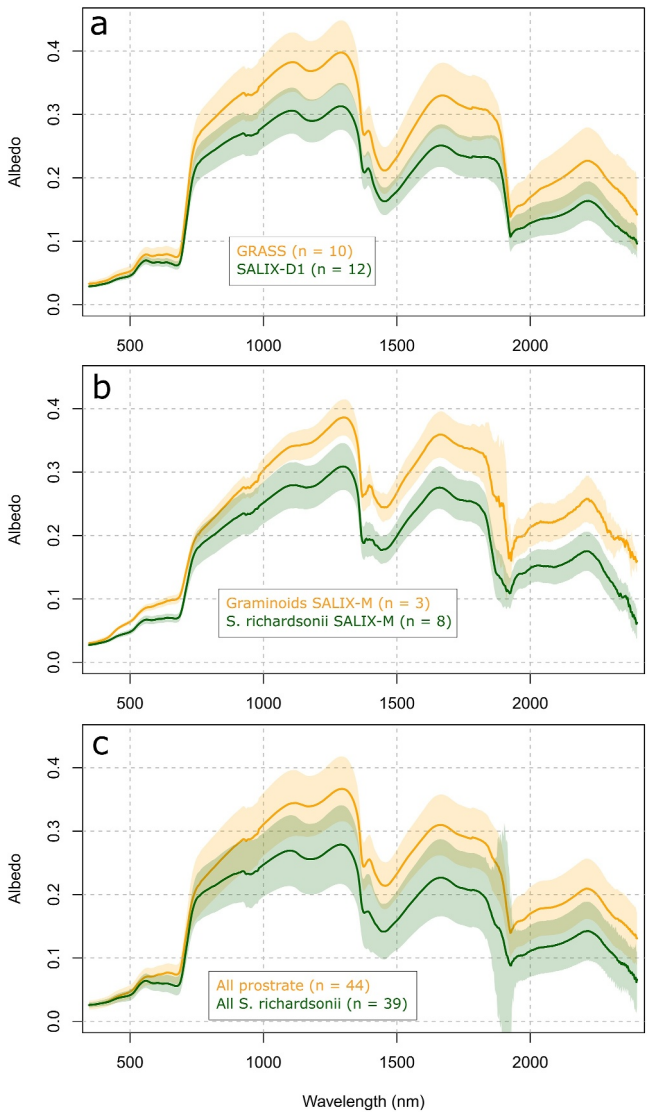

Figure 4. Comparisons of the average spectral albedos of prostrate vegetation with those of *Salix richardsonii* patches obtained under clear sky conditions. (a) at the SALIX-D1/GRASS sites, taken quasi-simultaneously under stable lighting conditions; (b) at the SALIX M site, under similar conditions to panel (a); (c) overall comparison of all the spectra. Shaded areas represent the standard deviation of all relevant spectra.

optimize the transect-areal agreement. With these limitations in mind, this approach was used to investigate the radiometric signal of pure stands of erect and prostrate vegetation at multiple scales.

3. Results

3.1. Field Spectral Albedo and NDVI

Figure 4 compares the spectral albedos of prostrate vegetation and of *S. richardsonii* patches. This shows that the spectral albedo is higher for prostrate vegetation than for *S. richardsonii* over the whole spectral range. This observation applies when comparing nearby pairs of sites (Figures 4a and 4b) and for the whole data set (Figure 4c). Notable different spectral features include a low albedo near 669 nm and a relatively low albedo at 1,300 nm for *S. richardsonii*. Overall, the BB albedo reduction is 0.032 under clear sky conditions and 0.027 under overcast conditions (Table 2). Figures 5c and 5d are graphical representations of Table 2, for easier visualization. The NDVI is lowest for soil (mudboils) and graminoids (0.501 and 0.517, respectively) and highest for *S. richardsonii* at the D1 and G2 sites (0.599 and 0.633, respectively), Table 2. However, overall, the NDVI difference between prostrate vegetation and *S. richardsonii* is very small (0.552 vs. 0.594) considering that the ranges of values largely overlap. In particular, it is noteworthy that the NDVI value for *S. richardsonii* at the mesic SALIX-M site, 0.517, is lower than the average value for mosses, 0.542 and also lower than the *S. arctica* average, 0.591. A large proportion of woody tissue (mostly pale gray, but with many reddish parts), few willow leaves and relatively dry mosses (brown) in the understory at the SALIX-M site may explain the low NDVI value (Figure S1 in Supporting Information S1).

Figure 5a illustrates the large variations in the spectral albedo of *S. richardsonii* between sites. The notably different spectral features from the SALIX-M location, in particular the high albedos around 669 and 1,300 nm, are probably due to a visibly lower LAI, which results in a greater contribution of understory species (Figure S1 in Supporting Information S1). The sandy soil at SALIX-M is also drier than the silty soils at SALIX-D1 and SALIX-G2. Since *S. richardsonii* tends to grow preferentially in moist areas, the SALIX-M location may not be a favorable site for optimal development. It is possible that *S. richardsonii* at SALIX-M is a relic from previous moister conditions.

Figure 5b reveals that, while spectral features are fairly similar for all prostrate vegetation types, there are significant differences in BB albedos (Figure 5c). The lowest BB albedo is for mudboil. It is important to note that mudboil spectra do not represent 100% bare soil, as mudboils are surrounded by prostrate vegetation (Figure S2 in Supporting Information S1).

3.2. Remote Sensing Reflectance and NDVI

Maps of NDVI values obtained with Landsat-8, Sentinel-2, Pléiades and the UAV are shown in Figure 3. The assignment of UAV and Pléiades pixels to *S. richardsonii* versus prostrate vegetation was performed with field transects (Figures 3c and 3d). Figure 6 shows reflectance values for the blue, green, red, red-edge and NIR UAV and Pléiades bands for *S. richardsonii* and prostrate vegetation. Numerical values of reflectances are detailed in Table S1 in Supporting Information S1. Differences between *S. richardsonii* and prostrate vegetation reflectances in the red (R) and NIR bands are very small, <0.005, for Pléiades. For the UAV data, however, it reaches 0.0098 for red-edge and 0.0127 in the NIR. A Wilcoxon rank sum test (Gibbons & Chakraborti, 2011) showed that these differences between vegetation types (*S.richardsonii* vs. prostrate) are statistically significant ($p < 0.01$) for all UAV bands, and for the red and NIR band for Pléiades-1B (Figure 7). However, differences are always very small

21698961, 2025, 10, Downloaded from https://agupubs.onlinelibrary.wiley.com/doi/10.1029/2024JG008593 by Universitaet Du Quebec A Trois Rivieres, Wiley Online Library on [11/02/2026]. See the Terms and Conditions (https://onlinelibrary.wiley.com/terms-and-conditions) on Wiley Online Library for rules of use; OA articles are governed by the applicable Creative Commons License

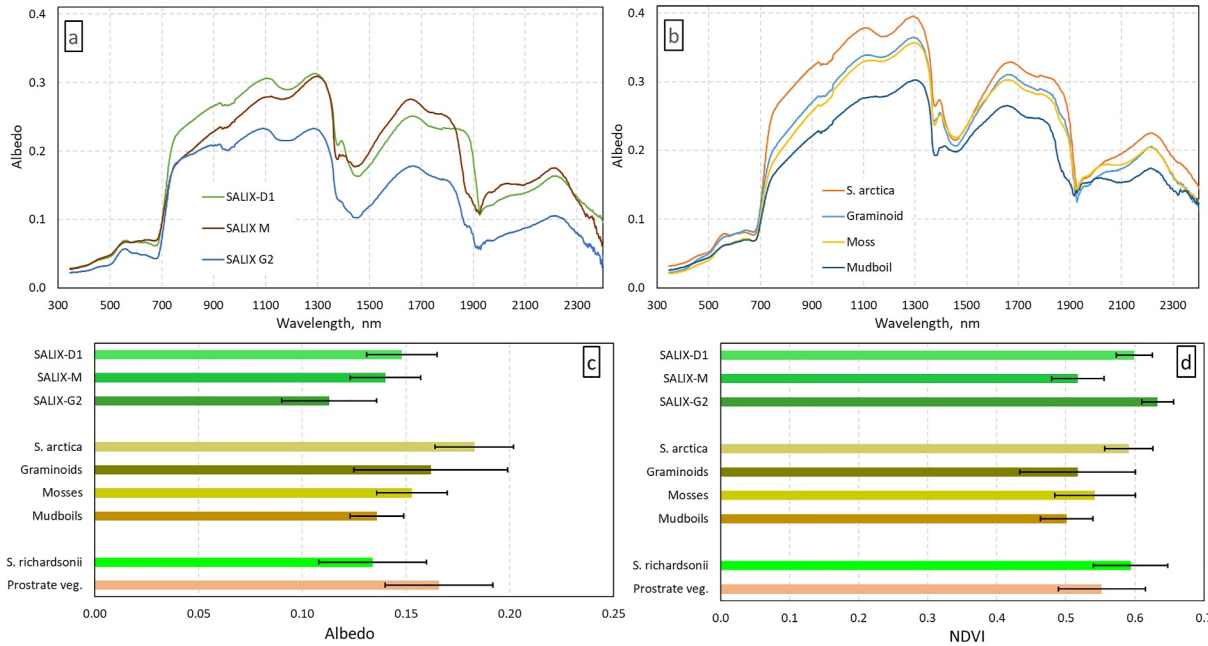

Figure 5. Spectral albedo, Broadband albedo and normalized difference vegetation index (NDVI) of the vegetation types studies. (a) Average spectral albedos for the three sites where *Salix richardsonii* was studied; (b) Average spectral albedo of the four types of prostrate vegetation studied, classified according to the dominant cover; (c) BB albedo and (d) NDVI of the cover types studied, with standard deviations as error bars. Average values for the main types (*S. richardsonii* and prostrate vegetation) are shown in the lower parts of (c) and (d).

compared to the spread of the values so that assigning a vegetation type based on reflectance is not possible. The distributions of NDVI values calculated from these reflectances are shown in Figure 7 for the UAV, Pléiades, Sentinel-2 and Landsat-8, with numerical values reported in Table S2 in Supporting Information S1. The median NDVI for *S. richardsonii* was slightly higher than for prostrate vegetation for the UAV and Pléiades 1B, by ~0.01 (Figures 7a and 7b). As for reflectance, the differences are very small in comparison to the range of variation within each type, so that reliably assigning a vegetation type from NDVI values is not possible. At a larger spatial scale, no significant difference in NDVI value is found for Landsat-8 and Sentinel-2 between both vegetation classes, corroborating results from Pléiades and UAV. The spectral bands do not cover a sufficient spectral range

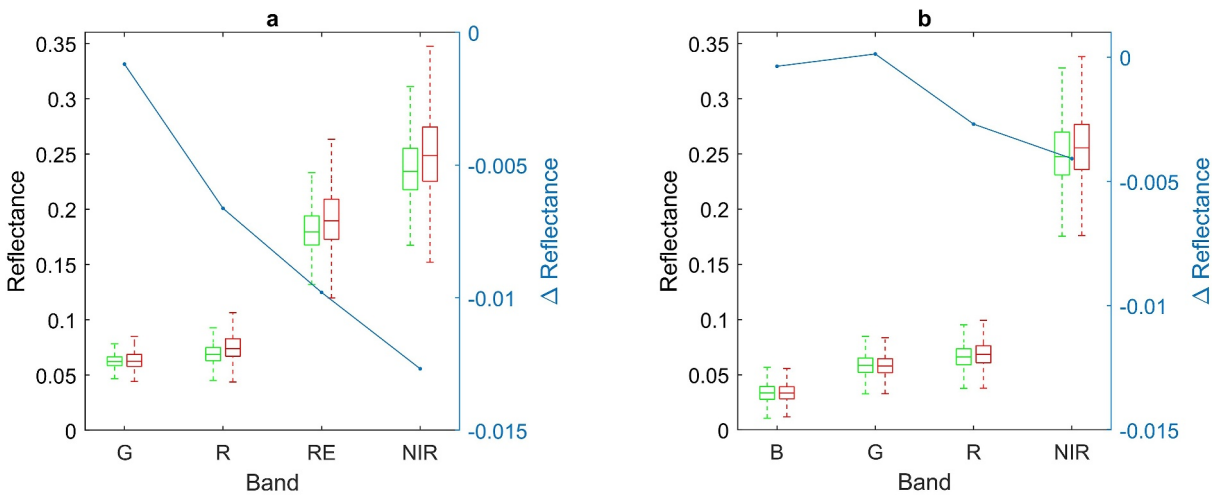

Figure 6. Difference in reflectance between *Salix richardsonii* (green) and prostrate (red) vegetation for (a) unmanned aerial vehicle and (b) Pléiades-1B (B: blue; G: green; R: red; RE: red-edge NIR: near-infrared). The difference between *S. richardsonii* and prostrate vegetation mean reflectance (Δ Reflectance) is displayed as a blue line on the right axis.

21698961, 2025, 10, Downloaded from https://agupubs.onlinelibrary.wiley.com/doi/10.1029/2024JG008593 by Universitaet Du Quebec A Trois Rivieres, Wiley Online Library on [11/02/2026]. See the Terms and Conditions (https://onlinelibrary.wiley.com/terms-and-conditions) on Wiley Online Library for rules of use; OA articles are governed by the applicable Creative Commons License

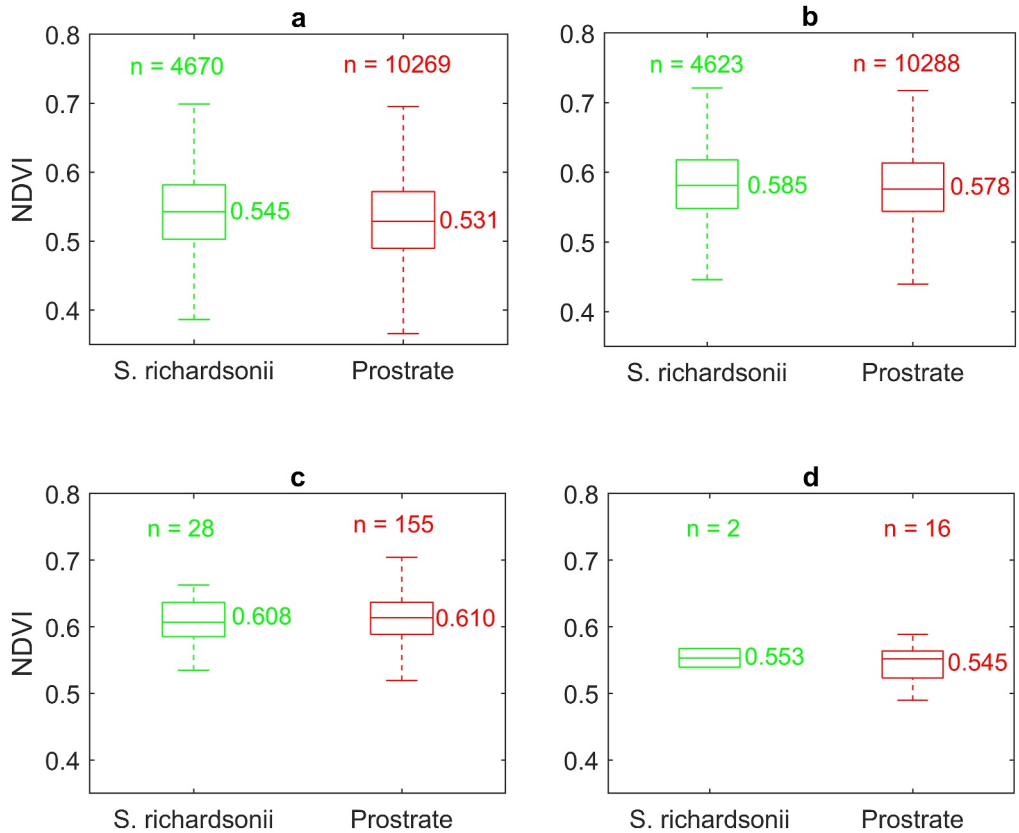

Figure 7. Difference in normalized difference vegetation index (NDVI) for *Salix richardsonii* shrubs (green) and prostrate vegetation (red) for (a) unmanned aerial vehicle, (b) Pléiades-1B, (c) Sentinel-2 and (d) Landsat 8. Median NDVI values are displayed on the plot along with the number of pixels considered.

for the reliable calculation of the BB albedo, so that a discussion on BB albedo that would be derived from remote sensing is not possible.

Figures 5a and 5d indicate that the larger shrub patches at SALIX-G2 have different spectral characteristics and higher NDVI values than the smaller patches at SALIX-D1. Earlier studies also noted an adjacency effect where patch size could affect reflectance (Richter, Bachmann, et al., 2006). We therefore tested the effect of patch size on UAV and Pléiades-1B data. Figure S8 in Supporting Information S1 shows no detectable effect.

Since these data indicate that NDVI and reflectance values cannot be used for differentiating *S. richardsonii* patches from prostrate vegetation in the high-Arctic valley studied, a legitimate question is whether this conclusion may be applied to the whole Canadian high-Arctic. While similar spectroscopic studies in numerous sites are required to address this question with certainty, a first partial response was obtained by determining the NDVI from Sentinel-2 over the whole Canadian high-Arctic, that is, climate zone C after (Walker et al., 2005). Figure 8 shows the results for July, based on 2017–2023 data. This is a composite image and data are not for the same day of July for all pixels. The bottom map of Figure 8 selects data for NDVI values >0.48. This is equivalent to a NDVI value of 0.49 obtained by our field spectroscopic studies because Sentinel-2 uses slightly different spectral ranges for its *R* and NIR bands. This threshold was chosen to be reasonably certain to detect even the *S. richardsonii* patches with the lowest NDVI values (Table 2). The area concerned with this NDVI limit covers 21,300 km^2. If our Bylot results can be extrapolated to the whole Canadian climate zone C, this means that the rest of climate zone C (2,253,160 km^2) is unlikely to host erect shrubs, and that in the 21,300 km^2 portion where erect shrub presence is possible, their presence cannot be established. To place this area in perspective, this area is about twice the size of Bylot Island and slightly larger than Lake Ontario. Based on the monitoring of downwelling shortwave radiation at Bylot Island (Domine et al., 2021), a BB albedo difference of 0.03 produces an average

21698961, 2025, 10, Downloaded from https://agupubs.onlinelibrary.wiley.com/doi/10.1029/2024JG008593 by Universitaet Du Quebec A Trois Rivieres, Wiley Online Library on [11/02/2026]. See the Terms and Conditions (https://onlinelibrary.wiley.com/terms-and-conditions) on Wiley Online Library for rules of use; OA articles are governed by the applicable Creative Commons License

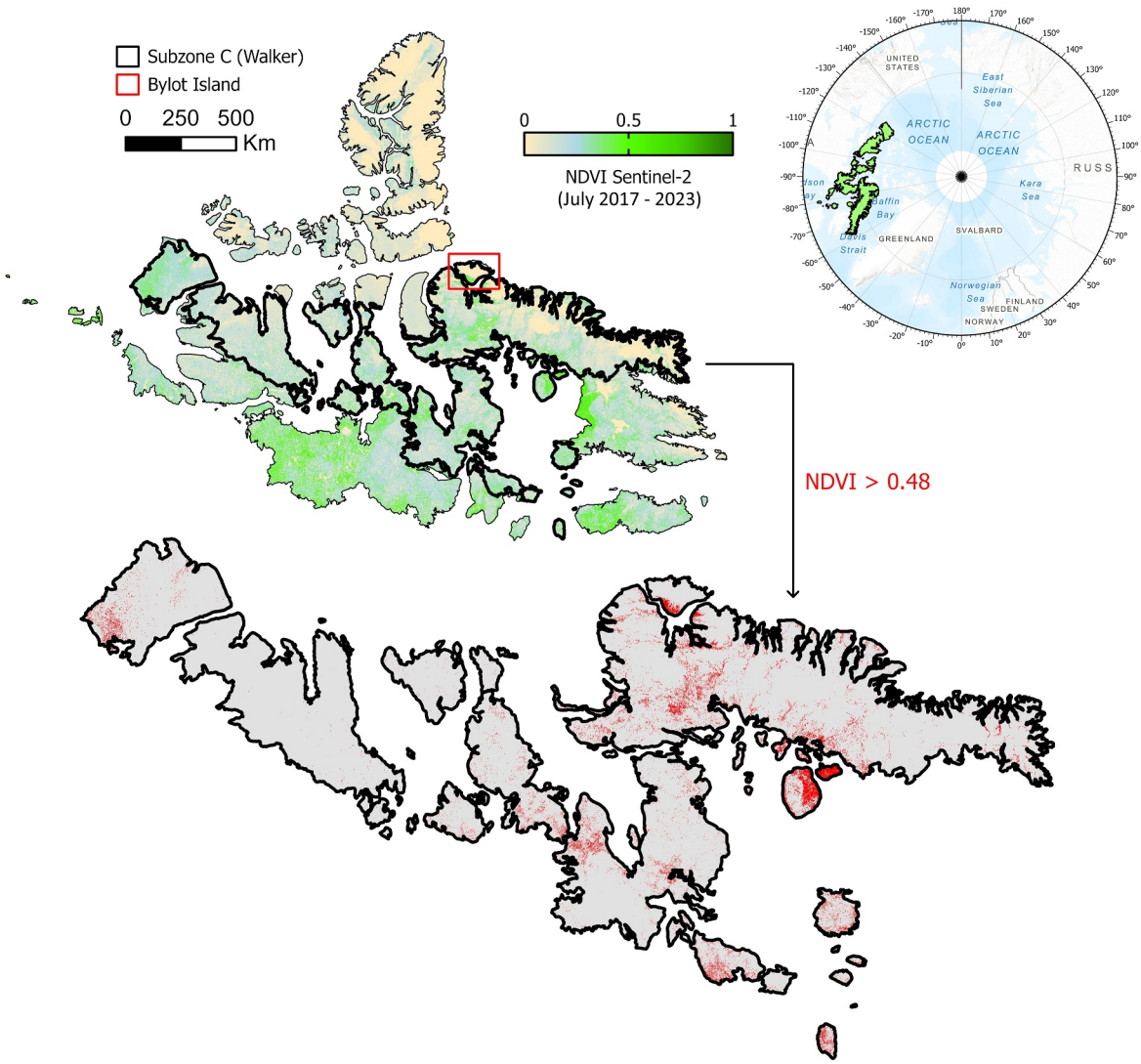

Figure 8. (Top) Normalized difference vegetation index (NDVI) values derived from Sentinel-2 data in July for the climate zones A, B, C, D of Walker et al. (2005) for the Canadian Arctic. Zone C (High-Arctic) where our study was located is delimited by a dark contour. (Bottom) Pixels with NDVI > 0.48 for climate zone C are shown in red. Climate zone C is highlighted on the general Arctic map, top right.

summer shortwave local forcing of a 5.8 W m^{-2}, based on data from the 2014–2018 period. This forcing may therefore be missed over a fraction of this 21,300 km^2 area. This fraction is likely to increase over time.

4. Discussion

Across the range of vegetation types sampled, the lowest BB albedo is for 50 cm tall shrub patches of *S. richardsonii* at the SALIX-G2 site, and the highest value is for surfaces dominated by prostrate *S. arctica* (Table 2, Figure 5c). The maximum BB albedo difference between prostrate vegetation and *S. richardsonii* is therefore 0.070 for clear sky conditions and 0.061 for overcast ones. Overall, the albedo difference between *S. richardsonii* and prostrate vegetation is 0.027–0.032, depending on lighting conditions. This is much less than observed in low-Arctic or boreal studies (Aartsma et al., 2020; Beringer et al., 2005; Blok et al., 2011; Nicholls & Carey, 2021; Ramtvedt et al., 2021), where differences sometimes exceeded 0.13. Since the BB albedo ranges show a large overlap, reliably differentiating *S. richardsonii* versus prostrate vegetation from albedo does not seem possible in most cases (Figure 5c). This can probably be explained by the presence here of only short-stature *S. richardsonii* patches with low LAI, which do not form a full canopy. The difference in albedo averaged over all our measurements nevertheless exists and produces a summer shortwave local forcing of 5.8 W m^{-2}. This is much

21698961, 2025, 10, Downloaded from https://agupubs.onlinelibrary.wiley.com/doi/10.1029/2024JG008593 by Universitaet Du Quebec A Trois Rivieres, Wiley Online Library on [11/02/2026]. See the Terms and Conditions (https://onlinelibrary.wiley.com/terms-and-conditions) on Wiley Online Library for rules of use; OA articles are governed by the applicable Creative Commons License

21698961, 2025, 10, Downloaded from https://agupubs.onlinelibrary.wiley.com/doi/10.1029/2024JG008593 by Universitaet Du Quebec A Trois Rivieres, Wiley Online Library on [11/02/2026]. See the Terms and Conditions (https://onlinelibrary.wiley.com/terms-and-conditions) on Wiley Online Library for rules of use; OA articles are governed by the applicable Creative Commons License

less than the difference between erect shrub and prostrate vegetation in the low-Arctic, or as calculated by models. For example (Domine, Bayle, et al., 2025), measured a forcing of 11.17 W m^{-2} for the replacement of lichen by dwarf birch in northern Quebec. Bonfils et al. (2012) determined using simulations that even for short shrubs, the shortwave forcing would exceed 20 W m^{-2} in summer. High-Arctic shrubification may therefore produce a more limited summer shortwave forcing, which should be considered by models.

In the UAV data, both ranges of reflectance values completely overlap, so that it is not possible to assign a given measured reflectance to one vegetation type or the other. The same conclusion applies to the Pléiades data. For field measurements, the overlap is much less so that some discrimination of the vegetation type may be possible in this case. The interest is however limited because simple field observations suffice to detect shrub presence. Besides the more complete spectral data provided by field measurements, a possible explanation for the better discriminating potential of field measurement may be the more specific footprint. The coarser Pléiades resolution may result in the inclusion of small areas of prostrate vegetation at pixel borders, and also possibly in a mix of vegetation types in a given pixel, increasing reflectance and decreasing the difference in value between both vegetation types. Field data on the contrary may be unconsciously biased, because operators wishing to measure shrubs inevitably place the integrating sphere over the thickest part of the patch and avoid small shrub gaps which are ubiquitous, and which the UAV does not avoid. UAV and satellite images are further affected by blurring due to the spatial point-spread function of the sensor, which leads to pixels neighboring a punctual target to contribute to the target reflectance (e.g., Huang et al., 2002).

NDVI values calculated from field spectra show a very limited range and the ranges strongly overlap among vegetation types (Figure 5d). This is corroborated by all the remote sensing data (Figure 7), with which it is in fact impossible to differentiate *S. richardsonii* from prostrate vegetation. This contrasts with the numerous low-Arctic studies (Berner et al., 2018; Blok et al., 2011; Fraser et al., 2014; Jespersen et al., 2023; Juszak et al., 2014; Myers-Smith et al., 2020; Pattison et al., 2015; Stow et al., 1993) which all observed that increased shrub cover led to an increase in NDVI, up to 0.80, while our highest average is 0.63, at SALIX-G2.

The explanation may be due to the shrub structure. The dominant shrub species in most of the low-Arctic studies were birch (*Betula nana* and *B. glandulosa*) and willow (*Salix pulchra*, *S. glauca*, and *S. richardsonii*) species, with a fairly dense canopy and a LAI usually greater than 1 (Berner et al., 2015; Myers-Smith, Hik, et al., 2011). Woody stems are therefore less visible. Here, *S. richardsonii* had few leaves and numerous visible woody stems (Figure S1 in Supporting Information S1). Boelman et al. (2011) showed that an increase in woody stem abundance led to a decrease in NDVI, down to values as low as 0.35. The abundance of woody stems, combined with the visibility of understory vegetation such as mosses of moderate NDVI (Figure 5d) is a likely explanation for the low shrub NDVI values we observed. The spatial variations in NDVI shown in Figure 3d may thus not be interpreted as due to *S. richardsonii* presence, as confirmed by Figure S7b in Supporting Information S1. Many pixels with high NDVI are prostrate vegetation, and these could possibly be dominated by *S. arctica*, which has NDVI values similar to and sometimes higher than *S. richardsonii*. At Herschel Islands, where *S. richardsonii* appears to have a slightly higher LAI than at our site based on published photographs, it is also difficult to identify this shrub using NDVI (Cunliffe et al., 2020). The problem of *S. richardsonii* detection using NDVI may therefore exist in large parts of the Arctic.

NDVI and albedo have been observed to be anticorrelated in low-Arctic studies (Blok et al., 2011; Juszak et al., 2014). Therefore, increases in NDVI observed using satellite remote sensing may be used to infer decreases in albedo. This is useful to force land surface models and evaluate the energy budget effects of vegetation changes. In our case, following this approach will imply that no albedo change takes place, since no difference in NDVI is observed (Figure 7) while in fact an albedo change of about 0.03 and a summer local forcing of 5.8 W m^{-2} are observed. This confusion may affect an area greater than 20,000 km^2 (Figure 8), which is likely to increase with the progression of greening. Missing this forcing will negatively impact the quality of land surface model outputs.

We therefore conclude that, contrary to the low-Arctic, neither reflectance nor NDVI values from field or remote sensing measurements can be reliably used to differentiate erect from prostrate vegetation at our high-Arctic study site. In the Canadian high-Arctic, the expansion of *S.richardsonii* at the expense of prostrate vegetation may not manifest itself as greening trends, and thus may go undetected. Detecting the spread of *S. richardsonii* using NDVI may therefore be unfeasible, leaving the associated 0.03 reduction in albedo unnoticed. Another formulation of this conclusion is that the absence of detection of *S. richardsonii* expansion there does not mean it is not

21698961, 2025, 10, Downloaded from https://agupubs.onlinelibrary.wiley.com/doi/10.1029/2024JG008593 by Universitaet Du Quebec A Trois Rivieres, Wiley Online Library on [11/02/2026]. See the Terms and Conditions (https://onlinelibrary.wiley.com/terms-and-conditions) on Wiley Online Library for rules of use; OA articles are governed by the applicable Creative Commons License

actually taking place. This impacts the validation of energy budget calculations by land surface models, as well as our ability to describe ecological changes and their implications.

To address the limitations of NDVI identified in this study, an alternative approach used successfully in the low-Arctic (Domine, Bayle, et al., 2025) is to use visible, NIR and SWIR satellite bands, and to train an algorithm with field spectral data to identify *S. richardsonii*. This is probably possible because this shrub has spectral characteristics significantly different to those of prostrate vegetation (Figure 4). Integrating refined remote sensing data with ground-based spectral measurements may therefore be a promising avenue. However, an extra difficulty will be to check that spectral data obtained at one location can be used at other locations. Training an identification model teaches this model to differentiate between several vegetation assemblages. These assemblages vary with soil type, moisture, climate, etc., so that numerous field studies recording spectral albedos may be required for this approach to be applicable to most of the Arctic.

Conflict of Interest

The authors declare no conflicts of interest relevant to this study.

Data Availability Statement

The spectral data of Figures 4 and 5; Figure S6 in Supporting Information S1 are available in the Zenodo repository (Domine et al., 2023). The 83 individual spectra obtained in this study are available in the Zenodo repository (Domine, Belke-Brea, et al., 2025). Photographs of 81 of the 83 vegetation assemblages where spectral albedos were recorded are available in the Zenodo repository (Belke-Brea & Domine, 2025).

Acknowledgments
This work was funded by the BNP-Paribas foundation (APT project to FD), the Natural Sciences and Engineering Research Council of Canada (Discovery Grant and Northern Research supplement programs to FD and CK), the French Polar Institute (IPEV, program 1042 to FD) and the Fonds de Recherche du Québec (FRQ). Logistical support was provided by the Polar Continental Shelf Program and by Sirmilik National Park to FD and CK. We thank Mathieu Barrère for help with field measurements. We are grateful to Gilles Gauthier and Marie-Christine Cadieux for their decades-long efforts to build and maintain the research base of the Centre d'Études Nordiques at Bylot Island. We thank Parks Canada and the community of Mittimatalik (Pond Inlet) for permission to perform the research, under permits SIR-2015-18616 (FD) and SIR-2021-39579 (CK).

References

Aartsma, P., Asplund, J., Odland, A., Reinhardt, S., & Renssen, H. (2020). Surface albedo of alpine lichen heaths and shrub vegetation. *Arctic Antarctic and Alpine Research*, *52*(1), 312–322. https://doi.org/10.1080/15230430.2020.1778890

Bayle, A., Roy, A., Dedieu, J.-P., Boudreau, S., Choler, P., & Lévesque, E. (2022). Two distinct waves of greening in northeastern Canada: Summer warming does not tell the whole story. *Environmental Research Letters*, *17*(6), 064051. https://doi.org/10.1088/1748-9326/ac74d6

Belke-Brea, M., & Domine, F. (2025). Photographs of vegetation assemblages from Bylot Island, Canadian high-Arctic, used for spectral albedo measurements [Dataset]. Zenodo. http://doi.org/10.5281/zenodo.15277241

Belke-Brea, M., Domine, F., Barrere, M., Picard, G., & Arnaud, L. (2020). Impact of shrubs on winter surface albedo and snow specific surface area at a low Arctic site: In situ measurements and simulations. *Journal of Climate*, *33*(2), 597–609. https://doi.org/10.1175/jcli-d-19-0318.1

Beringer, J., Chapin, F. S., Thompson, C. C., & McGuire, A. D. (2005). Surface energy exchanges along a tundra-forest transition and feedbacks to climate. *Agricultural and Forest Meteorology*, *131*(3), 143–161. https://doi.org/10.1016/j.agrformet.2005.05.006

Berner, L. T., Alexander, H. D., Loranty, M. M., Ganzlin, P., Mack, M. C., Davydov, S. P., & Goetz, S. J. (2015). Biomass allometry for alder, dwarf birch, and willow in boreal forest and tundra ecosystems of far northeastern Siberia and North-Central Alaska. *Forest Ecology and Management*, *337*, 110–118. https://doi.org/10.1016/j.foreco.2014.10.027

Berner, L. T., Jantz, P., Tape, K. D., & Goetz, S. J. (2018). Tundra plant above-ground biomass and shrub dominance mapped across the North Slope of Alaska. *Environmental Research Letters*, *13*(3), 035002. https://doi.org/10.1088/1748-9326/aaaa9a

Berner, L. T., Massey, R., Jantz, P., Forbes, B. C., Macias-Fauria, M., Myers-Smith, I., et al. (2020). Summer warming explains widespread but not uniform greening in the Arctic tundra biome. *Nature Communications*, *11*(1), 4621. https://doi.org/10.1038/s41467-020-18479-5

Bliss, L. C., & Matveyeva, N. V. (1992). Circumpolar Arctic vegetation. In F. S. Chapin III, R. L. Jefferies, J. F. Reynolds, G. R. Shaver, & J. Svoboda (Eds.), *Arctic ecosystems in a changing climate: An ecophysiological perspective* (pp. 59–89). Academic Press.

Blok, D., Schaepman-Strub, G., Bartholomeus, H., Heijmans, M. M. P. D., Maximov, T. C., & Berendse, F. (2011). The response of Arctic vegetation to the summer climate: Relation between shrub cover, NDVI, surface albedo and temperature. *Environmental Research Letters*, *6*(3), 035502. https://doi.org/10.1088/1748-9326/6/3/035502

Boelman, N. T., Gough, L., McLaren, J. R., & Greaves, H. (2011). Does NDVI reflect variation in the structural attributes associated with increasing shrub dominance in Arctic tundra? *Environmental Research Letters*, *6*(3), 035501. https://doi.org/10.1088/1748-9326/6/3/035501

Bonfils, C. J. W., Phillips, T. J., Lawrence, D. M., Cameron-Smith, P., Riley, W. J., & Subin, Z. M. (2012). On the influence of shrub height and expansion on northern high latitude climate. *Environmental Research Letters*, *7*(1), 015503. https://doi.org/10.1088/1748-9326/7/1/015503

Buchkowski, R. W., Morris, D. W., Halliday, W. D., Dupuch, A., Morrissette-Boileau, C., & Boudreau, S. (2020). Warmer temperatures promote shrub radial growth but not cover in the central Canadian Arctic. *Arctic Antarctic and Alpine Research*, *52*(1), 582–595. https://doi.org/10.1080/15230430.2020.1824558

Chang, Q. Y., Zwieback, S., De Vries, B., & Berg, A. (2022). Application of L-band SAR for mapping tundra shrub biomass, leaf area index, and rainfall interception. *Remote Sensing of Environment*, *268*, 268. https://doi.org/10.1016/j.rse.2021.112747

Chen, J., Zhang, Q., Kjellström, E., Lu, Z. Y., & Chen, F. H. (2022). The contribution of vegetation-climate feedback and resultant sea ice loss to amplified Arctic warming during the mid-holocene. *Geophysical Research Letters*, *49*(18), e2022GL098816. https://doi.org/10.1029/2022gl098816

Chen, T., de Jeu, R. A. M., Liu, Y. Y., van der Werf, G. R., & Dolman, A. J. (2014). Using satellite based soil moisture to quantify the water driven variability in NDVI: A case study over mainland Australia. *Remote Sensing of Environment*, *140*, 330–338. https://doi.org/10.1016/j.rse.2013.08.022

Colin, J., Hagolle, O., Landier, L., Coustance, S., Kettig, P., Meygret, A., et al. (2023). Assessment of the performance of the atmospheric correction algorithm MAJA for sentinel-2 surface reflectance estimates. *Remote Sensing*, *15*(10), 2665. https://doi.org/10.3390/rs15102665

Cubero-Castan, M., Schneider-Zapp, K., Bellomo, M., Shi, D., Rehak, M., Strecha, C., & IEEE. (2018). Assessment of the radiometric accuracy in a targetless workflow using PIX4D software, paper presented at 9th workshop on hyperspectral image and signal processing: Evolution in remote sensing (WHISPERS), Amsterdam, Netherlands, Sep 23–26.

Cunliffe, A. M., Assmann, J. J., Daskalova, G., Kerby, J. T., & Myers-Smith, I. H. (2020). Aboveground biomass corresponds strongly with drone-derived canopy height but weakly with greenness (NDVI) in a shrub tundra landscape. *Environmental Research Letters*, *15*(12), 125004. https://doi.org/10.1088/1748-9326/aba470

Domine, F., Barrere, M., & Morin, S. (2016). The growth of shrubs on high Arctic tundra at Bylot Island: Impact on snow physical properties and permafrost thermal regime. *Biogeosciences*, *13*(23), 6471–6486. https://doi.org/10.5194/bg-13-6471-2016

Domine, F., Bayle, A., Belke-Brea, M., Lévesque, E., & Picard, G. (2025). Quantified positive radiative forcing at a greening Canadian boreal-Arctic transition over the last four decades. *Remote Sensing of Environment*, *322*, 114715. https://doi.org/10.1016/j.rse.2025.114715

Domine, F., Belke-Brea, M., Picard, G., & Arnaud, L. (2023). Spectral albedo and summer ground temperature of herbaceous and shrub tundra vegetation at Bylot Island, Canadian high-Arctic [Dataset]. Zenodo. https://doi.org/10.5281/zenodo.10222606

Domine, F., Belke-Brea, M., Picard, G., & Arnaud, L. (2025). Spectral albedo of 83 vegetation assemblages on Bylot Island, Canadian high-Arctic [Dataset]. Zenodo. https://doi.org/10.5281/zenodo.15271811

Domine, F., Lackner, G., Sarrazin, D., Poirier, M., & Belke-Brea, M. (2021). Meteorological, snow and soil data (2013–2019) from a herb tundra permafrost site at Bylot Island, Canadian high Arctic, for driving and testing snow and land surface models. *Earth System Science Data*, *13*(9), 4331–4348. https://doi.org/10.5194/essd-13-4331-2021

Engstrom, R., Hope, A., Kwon, H., & Stow, D. (2008). The relationship between soil moisture and NDVI near Barrow, Alaska. *Physical Geography*, *29*(1), 38–53. https://doi.org/10.2747/0272-3646.29.1.38

Feister, U., & Grewe, R. (1995). Spectral albedo measurements in the UV and visible region over different types of surfaces. *Photochemistry and Photobiology*, *62*(4), 736–744. https://doi.org/10.1111/j.1751-1097.1995.tb08723.x

Forbes, B. C., Fauria, M. M., & Zetterberg, P. (2010). Russian Arctic warming and 'greening' are closely tracked by tundra shrub willows. *Global Change Biology*, *16*(5), 1542–1554. https://doi.org/10.1111/j.1365-2486.2009.02047.x

Fraser, R. H., Lantz, T. C., Olthof, I., Kokelj, S. V., & Sims, R. A. (2014). Warming-induced shrub expansion and lichen decline in the Western Canadian Arctic. *Ecosystems*, *17*(7), 1151–1168. https://doi.org/10.1007/s10021-014-9783-3

Frost, G. V., Bhatt, U. S., Macander, M. J., Berner, L. T., Walker, D. A., Raynolds, M. K., et al. (2025). The changing face of the Arctic: Four decades of greening and implications for tundra ecosystems. *Frontiers in Environmental Science*, *13*, 13–2025. https://doi.org/10.3389/fenvs.2025.1525574

Frost, G. V., & Epstein, H. E. (2014). Tall shrub and tree expansion in Siberian tundra ecotones since the 1960s. *Global Change Biology*, *20*(4), 1264–1277. https://doi.org/10.1111/gcb.12406

Gauthier, G., Berteaux, D., Bety, J., Tarroux, A., Therrien, J. F., McKinnon, L., et al. (2011). The tundra food web of Bylot Island in a changing climate and the role of exchanges between ecosystems. *Ecoscience*, *18*(3), 223–235. https://doi.org/10.2980/18-3-3453

Gauthier, G., Bety, J., Cadieux, M. C., Legagneux, P., Doiron, M., Chevallier, C., et al. (2013). Long-term monitoring at multiple trophic levels suggests heterogeneity in responses to climate change in the Canadian Arctic tundra. *Philosophical Transactions of the Royal Society B: Biological Sciences*, *368*(1624), 20120482. https://doi.org/10.1098/rstb.2012.0482

Gibbons, J. D., & Chakraborti, S. (2011). *Nonparametric statistical inference* (5th ed.). Chapman & Hall/CRC Press. https://doi.org/10.1111/j.1467-985X.2010.00681_6.x

González-Audícana, M., Otazu, X., Fors, O., & Seco, A. (2005). Comparison between Mallat's and the 'à trous' discrete wavelet transform based algorithms for the fusion of multispectral and panchromatic images. *International Journal of Remote Sensing*, *26*(3), 595–614. https://doi.org/10.1080/01431160512331314056

Huang, C. Q., Townshend, J. R. G., Liang, S. L., Kalluri, S. N. V., & DeFries, R. S. (2002). Impact of sensor's point spread function on land cover characterization: Assessment and deconvolution. *Remote Sensing of Environment*, *80*(2), 203–212. https://doi.org/10.1016/s0034-4257(01)00298-x

Jacobs, J. D., Headley, A. N., Maus, L. A., Mode, W. N., & Simms, E. L. (1997). Climate and vegetation of the interior lowlands of southern Baffin Island: Long-term stability at the low Arctic limit. *Arctic*, *50*(2), 167–177. https://doi.org/10.14430/arctic1099

Jespersen, R. G., Anderson-Smith, M., Sullivan, P. F., Dial, R. J., & Welker, J. M. (2023). NDVI changes in the Arctic: Functional significance in the moist acidic tundra of Northern Alaska. *PLoS One*, *18*(4), e0285030. https://doi.org/10.1371/journal.pone.0285030

Ju, J. C., & Masek, J. G. (2016). The vegetation greenness trend in Canada and US Alaska from 1984-2012 Landsat data. *Remote Sensing of Environment*, *176*, 1–16. https://doi.org/10.1016/j.rse.2016.01.001

Juszak, I., Erb, A. M., Maximov, T. C., & Schaepman-Strub, G. (2014). Arctic shrub effects on NDVI, summer albedo and soil shading. *Remote Sensing of Environment*, *153*, 79–89. https://doi.org/10.1016/j.rse.2014.07.021

Juszak, I., Iturrate-Garcia, M., Gastellu-Etchegorry, J. P., Schaepman, M. E., Maximov, T. C., & Schaepman-Strub, G. (2017). Drivers of shortwave radiation fluxes in Arctic tundra across scales. *Remote Sensing of Environment*, *193*, 86–102. https://doi.org/10.1016/j.rse.2017.02.017

Kropp, H., Loranty, M. M., Natali, S. M., Kholodov, A. L., Rocha, A. V., Myers-Smith, I., et al. (2021). Shallow soils are warmer under trees and tall shrubs across Arctic and Boreal ecosystems. *Environmental Research Letters*, *16*(1), 015001. https://doi.org/10.1088/1748-9326/abc994

Lafleur, P. M., & Humphreys, E. R. (2018). Tundra shrub effects on growing season energy and carbon dioxide exchange. *Environmental Research Letters*, *13*(5), 055001. https://doi.org/10.1088/1748-9326/aab863

Lamarque, L. J., Félix-Faure, J., Deschamps, L., Lévesque, E., Cusson, P. O., Fortier, D., et al. (2023). Hydrological regime and plant functional traits jointly mediate the influence of Salix spp. on soil organic carbon stocks in a high Arctic tundra. *Ecosystems*, *26*(6), 1238–1259. https://doi.org/10.1007/s10021-023-00829-1

Lebègue, L., Greslou, D., Blanchet, D., de Lssy, F., Fourest, F., Martin, V., et al. (2013). PLEIADES satellites image quality commissioning, paper presented at Earth Observing Systems XVIII. *SPIE Journals*, 8866.

May, J. L., Oberbauer, S. F., Unger, S. L., Simon, M. J., Betway, K. R., & Hollister, R. D. (2022). Shading decreases and delays NDVI and flowering of prostrate Arctic shrubs. *Arctic Science*, *8*(3), 967–978. https://doi.org/10.1139/as-2020-0043

Mekonnen, Z. A., Riley, W. J., Berner, L. T., Bouskill, N. J., Torn, M. S., Iwahana, G., et al. (2021). Arctic tundra shrubification: A review of mechanisms and impacts on ecosystem carbon balance. *Environmental Research Letters*, *16*(5), 053001. https://doi.org/10.1088/1748-9326/abf28b

Mohammadzadeh Khani, H., Kinnard, C., Gascoin, S., & Lévesque, E. (2023). Fine-scale environment control on ground surface temperature and thaw depth in a high Arctic tundra landscape. *Permafrost and Periglacial Processes*, *34*(4), 467–480. https://doi.org/10.1002/ppp.2203

Myers-Smith, I. H., Forbes, B. C., Wilmking, M., Hallinger, M., Lantz, T., Blok, D., et al. (2011). Shrub expansion in tundra ecosystems: Dynamics, impacts and research priorities. *Environmental Research Letters*, *6*(4), 045509. https://doi.org/10.1088/1748-9326/6/4/045509

21698961, 2025, 10, Downloaded from https://agupubs.onlinelibrary.wiley.com/doi/10.1029/2024JG008593 by Universitaet Du Quebec A Trois Rivieres, Wiley Online Library on [11/02/2026]. See the Terms and Conditions (https://onlinelibrary.wiley.com/terms-and-conditions) on Wiley Online Library for rules of use; OA articles are governed by the applicable Creative Commons License

Myers-Smith, I. H., Hallinger, M., Blok, D., Sass-Klaassen, U., Rayback, S. A., Weijers, S., et al. (2015). Methods for measuring Arctic and Alpine shrub growth: A review. *Earth-Science Reviews*, *140*, 1–13. https://doi.org/10.1016/j.earscirev.2014.10.004

Myers-Smith, I. H., Hik, D. S., Kennedy, C., Cooley, D., Johnstone, J. F., Kenney, A. J., & Krebs, C. J. (2011). Expansion of canopy-forming willows over the twentieth century on Herschel Island, Yukon Territory, Canada. *Ambio*, *40*(6), 610–623. https://doi.org/10.1007/s13280-011-0168-y

Myers-Smith, I. H., Kerby, J. T., Phoenix, G. K., Bjerke, J. W., Epstein, H. E., Assmann, J. J., et al. (2020). Complexity revealed in the greening of the Arctic. *Nature Climate Change*, *10*(2), 106–117. https://doi.org/10.1038/s41558-019-0688-1

Nicholls, E. M., & Carey, S. K. (2021). Evapotranspiration and energy partitioning across a forest-shrub vegetation gradient in a subarctic, alpine catchment. *Journal of Hydrology*, *602*, 126790. https://doi.org/10.1016/j.jhydrol.2021.126790

Ola, A., Fortier, D., Coulombe, S., Comte, J., & Domine, F. (2022). The distribution of soil carbon and nitrogen stocks among dominant geomorphological terrain units in Qarlikturvik Valley, Bylot Island, Arctic Canada. *Journal of Geophysical Research: Biogeosciences*, *127*(7), e2021JG006750. https://doi.org/10.1029/2021JG006750

Pattison, R. R., Jorgenson, J. C., Raynolds, M. K., & Welker, J. M. (2015). Trends in NDVI and Tundra Community composition in the Arctic of NE Alaska between 1984 and 2009. *Ecosystems*, *18*(4), 707–719. https://doi.org/10.1007/s10021-015-9858-9

Plekhanova, E., Kim, J.-S., Oehri, J., Erb, A., Schaaf, C., & Schaepman-Strub, G. (2022). Mid-summer snow-free albedo across the Arctic tundra was mostly stable or increased over the past two decades. *Environmental Research Letters*, *17*(12), 124026. https://doi.org/10.1088/1748-9326/aca5a1

Poirier, M., Gauthier, G., Domine, F., & Fauteux, D. (2023). Lemming winter habitat: The quest for warm and soft snow. *Oecologia*, *202*(2), 211–225. https://doi.org/10.1007/s00442-023-05385-y

Ramtvedt, E. N., Bollandsås, O. M., Næsset, E., & Gobakken, T. (2021). Relationships between single-tree mountain birch summertime albedo and vegetation properties. *Agricultural and Forest Meteorology*, *307*, 108470. https://doi.org/10.1016/j.agrformet.2021.108470

Rees, W. G., Golubeva, E. I., Tutubalina, O. V., Zimin, M. V., & Derkacheva, A. A. (2020). Relation between leaf area index and NDVI for subarctic deciduous vegetation. *International Journal of Remote Sensing*, *41*(22), 8573–8589. https://doi.org/10.1080/01431161.2020.1782505

Richter, R., Bachmann, M., Dorigo, W., & Muller, A. (2006). Influence of the adjacency effect on ground reflectance measurements. *IEEE Geoscience Remote Sensing Letters*, *3*(4), 565–569. https://doi.org/10.1109/LGRS.2006.882146

Richter, R., & Schläpfer, D. (2017). Atmospheric/Topographic correction for satellite imagery (ATCOR-2/3, Version 9.1.1, February 2017) theoretical background document.

Richter, R., Schläpfer, D., & Müller, A. (2006). An automatic atmospheric correction algorithm for visible/NIR imagery. *International Journal of Remote Sensing*, *27*(10), 2077–2085. https://doi.org/10.1080/01431160500486690

Ropars, P., & Boudreau, S. (2012). Shrub expansion at the forest-tundra ecotone: Spatial heterogeneity linked to local topography. *Environmental Research Letters*, *7*(1), 015501. https://doi.org/10.1088/1748-9326/7/1/015501

Rydsaa, J. H., Stordal, F., & Tallaksen, L. M. (2015). Sensitivity of the regional European boreal climate to changes in surface properties resulting from structural vegetation perturbations. *Biogeosciences*, *12*(10), 3071–3087. https://doi.org/10.5194/bg-12-3071-2015

Sandmeier, S. R., Middleton, E. M., Deering, D. W., & Qin, W. H. (1999). The potential of hyperspectral bidirectional reflectance distribution function data for grass canopy characterization. *Journal of Geophysical Research*, *104*(D8), 9547–9560. https://doi.org/10.1029/1999jd900094

Stow, D. A., Hope, A. S., & George, T. H. (1993). Reflectance characteristics of Arctic tundra vegetation from airborne radiometry. *International Journal of Remote Sensing*, *14*(6), 1239–1244. https://doi.org/10.1080/01431169308904408

Sturm, M., Racine, C., & Tape, K. (2001). Climate change. Increasing shrub abundance in the Arctic. *Nature*, *411*(6837), 546–547. https://doi.org/10.1038/35079180

te Beest, M., Sitters, J., Menard, C. B., & Olofsson, J. (2016). Reindeer grazing increases summer albedo by reducing shrub abundance in Arctic tundra. *Environmental Research Letters*, *11*(12), 125013. https://doi.org/10.1088/1748-9326/aa5128

Walker, D. A., Raynolds, M. K., Daniëls, F. J., Einarsson, E., Elvebakk, A., Gould, W. A., et al. (2005). The circumpolar Arctic vegetation map. *Journal of Vegetation Science*, *16*(3), 267–282. https://doi.org/10.1111/j.1654-1103.2005.tb02365.x

Webb, E. E., Loranty, M. M., & Lichstein, J. W. (2021). Surface water, vegetation, and fire as drivers of the terrestrial Arctic-boreal albedo feedback. *Environmental Research Letters*, *16*(8), 084046. https://doi.org/10.1088/1748-9326/ac14ea

Yu, L., Leng, G., & Python, A. (2022). Attribution of the spatial heterogeneity of Arctic surface albedo feedback to the dynamics of vegetation, snow and soil properties and their interactions. *Environmental Research Letters*, *17*(1), 014036. https://doi.org/10.1088/1748-9326/ac4631

21698961, 2025, 10, Downloaded from https://agupubs.onlinelibrary.wiley.com/doi/10.1029/2024JG008593 by Universitaet Du Quebec A Trois Rivieres, Wiley Online Library on [11/02/2026]. See the Terms and Conditions (https://onlinelibrary.wiley.com/terms-and-conditions) on Wiley Online Library for rules of use; OA articles are governed by the applicable Creative Commons License